Scaling Laws, Poverty Traps, and the UrbanizationCrossover in Chinese County Economies

Juk-Sen Tang *

Posted Date: 5 March 2026

doi: 10.20944/preprints202603.0443.v1

Keywords: scaling laws; urbanization crossover; poverty traps; county economies; interaction-term regression; China

 doi:10.20944/preprints202603.0443.v1

Article

Scaling Laws, Poverty Traps, and the Urbanization Crossover in Chinese County Economies

Juk-Sen Tang

Department of Agricultural Economics, MacDonald Campus, McGill University, Montréal, Québec, H9X 3V9, Canada; juksen.tang@mail.mcgill.ca

Abstract

Urban scaling theory establishes that socioeconomic outputs scale superlinearly with city population ($\beta > 1$), attributed to social-interaction density, but its applicability to resource-constrained sectors remains untested. We analyse a panel of $\sim$2,800 Chinese counties (2000–2023) with GDP decomposed into primary, secondary, and tertiary sectors. Using the urbanization ratio as a continuous moderator in interaction-term regressions, we estimate sector-specific crossover thresholds from sub- to superlinear scaling; a Scale-Adjusted Agricultural Index (SAAI) quantifies each county's deviation from size-expected output. A robust sectoral spectrum emerges—$\beta_{\text{pri}} = 0.87 < \beta_{\text{ter}} = 0.96 < \beta_{\text{sec}} = 1.08$—whose rank order is preserved across all 24 sample years. The tertiary sector crosses $\beta = 1$ at urbanization ratio $u^* = 0.80$ (95% CI [0.72, 0.92]), with interaction coefficient $\beta_1 = 1.48$ ($p < 0.001$). Province fixed effects confirm the urbanization interaction for secondary and tertiary sectors ($p < 0.001$) but not primary ($p = 0.248$), consistent with the crossover being specific to interaction-intensive activities. China's 832 designated poverty counties exhibit systematically negative SAAI values (Cohen's $d = 0.55$–0.87), revealing a persistent scaling deficit that conventional output comparisons obscure. These results show that the scaling exponent is a continuous function of economic structure, identify a quantifiable urbanization threshold for the onset of increasing returns, and supply a boundary condition for Bettencourt's theory of urban scaling.

Keywords: scaling laws; urbanization crossover; poverty traps; county economies; interaction-term regression; China

1. Introduction

Across urban systems worldwide, aggregate socioeconomic outputs obey a remarkably simple regularity: total output Y scales as a power law of city population N,

$$Y \sim N^{\beta}, \tag{1}$$

where the exponent β partitions urban phenomena into two classes. Quantities that reflect the intensity of social interaction—gross domestic product, patent output, total wages, serious crime—scale *superlinearly* ($\beta \approx 1.15$), while material infrastructure—road surface, electrical cable length, petrol stations—scales *sublinearly* ($\beta \approx 0.85$) (Bettencourt et al., 2007a). The regularity has been replicated for cities in the United States, Europe, Brazil, and China, spanning population sizes from 10^4 to 10^7. Bettencourt (2013) traced the origin of superlinear scaling to a micro-level mechanism: in a bounded area, N individuals generate $\mathcal{O}(N^2)$ pairwise encounters whose frequency grows faster than N, producing knowledge spillovers and increasing returns to agglomeration. The critical assumption is that output is proportional to the total volume of these social interactions, so that doubling the population more than doubles the output. Direct empirical support followed from Schläpfer et al. (2014), who showed that per-capita mobile-phone contacts indeed increase with city size at a rate quantitatively consistent with the predicted interaction frequency. The sublinear branch has a parallel

 doi:10.20944/preprints202603.0443.v1

genealogy: hierarchical resource-distribution networks—first formalised for biological metabolic systems by West et al. (1997)—impose economies of scale on infrastructure, yielding $\beta < 1$. Together, the super- and sublinear exponents define what Bettencourt et al. (2016) call the "urban scaling hypothesis": a universal statistical signature of how cities organise production and allocate resources.

Yet nearly all tests of this hypothesis share two limitations. First, the spatial units are cities or metropolitan areas; whether scaling regularities extend to rural counties—where population densities are lower by an order of magnitude and a large fraction of residents engage in agricultural rather than knowledge-intensive occupations—remains untested. Second, the dependent variable is almost always aggregate GDP or a single composite indicator; whether *different economic sectors within the same spatial unit* obey the same exponent has received little systematic attention. This omission matters because the interaction mechanism invoked by Bettencourt (2013) is specific to knowledge-intensive activities. Agricultural production, by contrast, is fundamentally a human–resource interaction: output depends on the quantity and quality of arable land, water availability, and sunlight, not on the frequency with which farmers exchange ideas in market squares. If superlinear scaling truly originates in pairwise social interaction, then sectors that do not rely on that mechanism—above all, primary agriculture—should *not* exhibit $\beta > 1$, regardless of population size. A theoretical prediction follows: among the three broad sectors, exponents should be ordered by the sector's dependence on human–human interaction, with primary agriculture lowest and services or manufacturing highest.

Two methodological concerns sharpen the gap. Arcaute et al. (2015) showed that estimated exponents are sensitive to how spatial units are delineated, raising the question of whether administratively defined counties yield meaningful scaling at all. Leitão et al. (2016) demonstrated that conventional log–log regressions can overstate nonlinearity unless null hypotheses are carefully specified. These critiques call for a setting in which the same units host both interaction-driven and resource-constrained sectors, enabling a within-unit comparison that side-steps boundary and aggregation artefacts.

Here we show that, across $\sim$2,800 Chinese counties observed annually from 2000 to 2023, the scaling exponent is *not* a universal constant but varies systematically with the sector's reliance on social interaction. Three layers of evidence support this conclusion.

First, a stable *sectoral spectrum* of exponents emerges: $\beta_{\text{pri}} = 0.87 < \beta_{\text{ter}} = 0.96 < \beta_{\text{sec}} = 1.08$, where subscripts denote primary, tertiary, and secondary GDP respectively. This rank order is preserved in every one of the 24 sample years and is robust to province fixed effects, alternative econometric specifications, and block-bootstrap inference. The ordering is consistent with a mechanism-based interpretation: secondary industry (manufacturing) involves the densest network of inter-firm supply chains and labour pooling, the tertiary sector relies on but is not exhausted by face-to-face interaction, and primary agriculture depends predominantly on natural-resource inputs.

Second, the *urbanization ratio*—defined as the share of non-agricultural GDP in total county GDP—acts as a continuous moderator of the exponent. An interaction-term regression of the form $\ln Y = \alpha + (\beta_0 + \beta_1 u) \ln N + \varepsilon$ reveals that $\beta_1 > 0$ and highly significant for secondary and tertiary sectors, but statistically indistinguishable from zero for primary agriculture. The tertiary sector crosses the linear benchmark $\beta(u^*) = 1$ at urbanization ratio $u^* = 0.80$ (95% CI [0.72, 0.92]); the secondary sector at $u^* \approx 0.75$; the primary sector exhibits no crossover at any urbanization level. Province fixed effects preserve these results ($p < 0.001$ for secondary and tertiary, $p = 0.248$ for primary), confirming that the crossover is not an artefact of regional heterogeneity.

Third, we define a *Scale-Adjusted Agricultural Index* (SAAI)—the standardised residual from the primary-sector scaling regression—and show that China's 832 nationally designated poverty counties exhibit systematically negative SAAI values (Cohen's $d = 0.55$–0.87 depending on year and specification), indicating a persistent scaling deficit that conventional output comparisons fail to detect. This finding connects the scaling framework to the poverty-trap literature (Azariadis and Stachurski, 2005; Barrett and Carter, 2013) and suggests that deviations from expected scaling behaviour can serve as a quantitative diagnostic of structural disadvantage. Taken together, these results imply that

 doi:10.20944/preprints202603.0443.v1

superlinearity is not an automatic consequence of population size but requires a sufficient density of knowledge-intensive economic activity—a threshold that the crossover point u^* quantifies.

China's county system provides an unusually suitable laboratory for these tests. The $\sim$2,800 county-level units span populations from fewer than 50 000 to more than 2 000 000, covering the full range from deeply rural to peri-urban economies. Because each unit reports GDP disaggregated into primary, secondary, and tertiary components—as well as agricultural gross output, cultivated area, and sown area—the data permit within-unit comparisons across production regimes without the need to match different data sources at different spatial scales. The 832 nationally designated poverty counties, whose official exit years range from 2016 to 2020 under the Targeted Poverty Alleviation campaign, provide a natural reference group for evaluating scaling anomalies (Liu et al., 2020). Finally, the 24-year panel (2000–2023) spans a period during which China's aggregate urbanization rate rose from 36% to 65%, generating substantial within-unit variation in the urbanization moderator and enabling identification of the crossover threshold from temporal as well as cross-sectional variation.

2. Theoretical Framework and Methods

2.1. Scaling Regression Framework

We estimate scaling exponents separately for each of the four output categories $s \in \{\text{Primary, Secondary, Tertiary, Non-agricultural}\}$. The baseline specification is a log-linear panel regression with year fixed effects:

$$\ln Y_{i,t}^{(s)} \;=\; \alpha_t \;+\; \beta^{(s)} \ln N_{i,t} \;+\; \varepsilon_{i,t}\,, \tag{2}$$

where $Y_{i,t}^{(s)}$ is the real output of sector s in county i and year t (deflated to 2000 prices), $N_{i,t}$ is the registered population, and α_t absorbs common year-level shocks such as macroeconomic cycles and national policy changes. All standard errors are heteroskedasticity-robust (HC1). A Wald test of $H_0\colon \beta^{(s)} = 1$ classifies each sector as superlinear ($\beta > 1$), sublinear ($\beta < 1$), or linear ($\beta = 1$).

For the primary sector, output may be constrained by a fixed natural input—land. To separate the population exponent from the land contribution, we augment the regression with a land area control:

$$\ln Y_{i,t}^{\text{agri}} \;=\; \alpha_t \;+\; \beta_N \ln N_{i,t} \;+\; \gamma \ln A_{i,t} \;+\; \varepsilon_{i,t}\,, \tag{3}$$

where $A_{i,t}$ denotes cultivated area (or, as a robustness check, total sown area). If the sublinearity identified in (2) reflects resource crowding—that is, too many workers sharing too little land—then β_N in (3) should fall below $\beta^{(\text{pri})}$ in (2), while $\gamma > 0$ captures the direct land contribution. As a placebo, we estimate the same specification with non-agricultural GDP as the dependent variable; the prediction is that β_N should remain unchanged, because non-agricultural output does not depend on arable land.

The central analytical tool is an interaction-term regression that allows the scaling exponent to vary continuously with the county's economic structure:

$$\ln Y_{i,t}^{(s)} \;=\; \alpha_t \;+\; \left(\beta_0 + \beta_1\, u_{i,t}\right) \ln N_{i,t} \;+\; \varepsilon_{i,t}\,, \tag{4}$$

where the urbanization ratio $u_{i,t} \equiv \text{NonAgriGDP}_{i,t} \,/\, \text{RegGDP}_{i,t}$ measures the share of economic activity outside agriculture. The effective scaling exponent is $\beta_{\text{eff}}(u) = \beta_0 + \beta_1\, u$, a linear function of u. When $\beta_1 > 0$, the exponent increases with urbanization; when $\beta_1 = 0$, urbanization has no moderating effect. The *crossover point*—the urbanization level at which scaling switches from sublinear to superlinear—is defined by $\beta_{\text{eff}}(u^*) = 1$, yielding

$$u^* = \frac{1 - \beta_0}{\beta_1}\,. \tag{5}$$

This threshold is estimated endogenously from the data rather than imposed by an arbitrary grouping of counties, which is the main advantage of the continuous interaction approach over discrete stratifi-

 doi:10.20944/preprints202603.0443.v1

cation. Our core prediction is that $\beta_1 > 0$ for secondary and tertiary sectors (whose output benefits from social-interaction intensity) and $\beta_1 \approx 0$ for the primary sector (whose output is land-constrained and interaction-insensitive).

To address the concern that the urbanization ratio may proxy for unobserved provincial-level endowments (e.g. geography, institutions, historical development), we re-estimate (4) with province fixed effects replacing the year fixed effects:

$$\ln Y_{i,t}^{(s)} \;=\; \alpha_j \;+\; \left(\beta_0 + \beta_1\, u_{i,t}\right) \ln N_{i,t} \;+\; \varepsilon_{i,t}\,, \tag{6}$$

where α_j absorbs all time-invariant differences across province j. If β_1 remains significant in (6), the urbanization effect operates *within* provinces and is not driven by between-province heterogeneity.

A further concern is that u and $\ln N$ may be correlated—larger counties tend to be more urbanised—so that the interaction term could spuriously reflect a nonlinear population-size effect rather than a genuine structural moderator. We therefore augment (4) with a quadratic population term:

$$\ln Y_{i,t} \;=\; \alpha_t \;+\; \left(\beta_0 + \beta_1\, u_{i,t} + \beta_2\, \ln N_{i,t}\right) \ln N_{i,t} \;+\; \varepsilon_{i,t}\,. \tag{7}$$

If β_1 survives this augmentation and u^* remains stable, the crossover is attributable to economic structure rather than to population scale per se.

2.2. Scale-Adjusted Agricultural Index

Following the logic of the Scale-Adjusted Metropolitan Indicator introduced by Bettencourt et al. (2007b) and Lobo et al. (2013)—which measures a city's deviation from expected output given its population—we define a county-level analogue that additionally controls for land endowment. The *Scale-Adjusted Agricultural Index* (SAAI) for county i in year t is the standardised residual from the multi-factor scaling regression (3):

$$\xi_{i,t} \;\equiv\; \frac{\ln Y_{i,t}^{\text{agri}} - \left(\hat{\alpha}_t + \hat{\beta}_N \ln N_{i,t} + \hat{\gamma}\, \ln A_{i,t}\right)}{\hat{\sigma}_t}\,, \tag{8}$$

where $\hat{\sigma}_t$ is the residual standard deviation in year t. By construction, $\xi_{i,t}$ has zero mean and unit variance within each year. A county with $\xi > 0$ produces more agricultural output than predicted by its population and land endowment; $\xi < 0$ indicates a systematic shortfall—an operationalisation of what the poverty-trap literature terms "being below the Micawber frontier" (Barrett and Carter, 2013).

Three versions of the SAAI are computed for robustness: a single-factor version controlling only for population, and two multi-factor versions using cultivated area and total sown area respectively. All three yield pairwise correlations above $r = 0.9$ (see Supplementary Information), confirming that the index is not sensitive to the choice of land variable.

2.3. Distributional Dynamics

To characterise the time evolution of the SAAI distribution, we adopt the Fokker–Planck formalism, which describes how a probability density $P(\xi, t)$ evolves under the combined influence of a deterministic drift $A(\xi)$ and a stochastic diffusion $B(\xi)$ (Risken, 1996):

$$\frac{\partial P}{\partial t} \;=\; -\frac{\partial}{\partial \xi}\left[A(\xi)\, P\right] \;+\; \frac{1}{2}\,\frac{\partial^2}{\partial \xi^2}\left[B(\xi)\, P\right]. \tag{9}$$

The drift $A(\xi)$ represents the systematic tendency of counties at position ξ to move up or down the SAAI scale; the diffusion $B(\xi)$ captures the amplitude of idiosyncratic shocks.

We estimate $A(\xi)$ and $B(\xi)$ from the Kramers–Moyal conditional moments (Friedrich et al., 2011):

$$A(\xi) = \frac{\langle \Delta\xi \rangle_\xi}{\Delta t}\,, \qquad B(\xi) = \frac{\langle (\Delta\xi)^2 \rangle_\xi}{\Delta t}\,, \tag{10}$$

 doi:10.20944/preprints202603.0443.v1

where $\Delta\xi = \xi_{i,t+1} - \xi_{i,t}$ is the one-year increment for county i, and the angle brackets denote conditional averages over all counties whose SAAI falls within a bin centred at ξ. The SAAI axis is partitioned into 25 equal-width bins; bins with fewer than 30 transition pairs are flagged as unreliable.

To allow for structural breaks associated with the Targeted Poverty Alleviation campaign (2013–2020), we pool transition pairs into three periods: *pre* (2000–2012), *during* (2013–2019), and *post* (2020–2023), and estimate separate drift and diffusion profiles for each.

The zeros of the drift function, $A(\xi^*) = 0$, identify the system's equilibrium points. A zero with $A'(\xi^*) < 0$ is a stable attractor: counties near ξ^* are drawn back to it. A zero with $A'(\xi^*) > 0$ is an unstable repeller: counties are pushed away in both directions. Multiple stable zeros indicate the coexistence of distinct equilibrium states in the SAAI distribution.

For a complementary, model-free characterisation, we also compute the effective potential directly from the stationary density (Kramers, 1940):

$$V_{\text{eff}}(\xi) \;=\; -\ln P(\xi) + C\,, \tag{11}$$

where C is an arbitrary constant. Local minima of V_{eff} correspond to modes of the density (stable states), and local maxima correspond to density troughs (barriers between states). The depth of a minimum relative to the adjacent maximum gives the "barrier height" that a county must stochastically overcome to transition between states.

As a validation exercise, we verify the Kramers–Moyal estimates by generating synthetic data from a Langevin equation with known drift and diffusion, then recovering the input parameters; details are reported in the Supplementary Information.

2.4. Data

Our data are drawn from the China County Statistical Database (version 6.0), which compiles annual socioeconomic indicators for all county-level administrative units. We restrict the sample to counties proper by retaining units whose six-digit administrative code satisfies code mod $100 \geq 21$, thereby excluding urban districts (codes 01–20). After this filter, the panel comprises approximately 2,800 counties observed annually from 2000 to 2023.

Variables. Gross domestic product is reported separately for primary, secondary, and tertiary sectors; we define non-agricultural GDP as the sum of secondary and tertiary. Population (N) is the year-end registered total (in units of 10 000 persons). Agricultural gross output value includes farming, forestry, animal husbandry, fishery, and services. Land variables include cultivated area (hectares) and total sown area (hectares); the latter has higher coverage ($\sim$62% vs. $\sim$45% for cultivated area). Grain output (tonnes) is used in a placebo test. The urbanization ratio u is computed as non-agricultural GDP divided by total regional GDP.

Deflation. All monetary variables are deflated to constant 2000 prices using provincial implicit GDP deflators constructed from nominal and real GDP indices.

Poverty designation. A total of 832 counties are nationally designated poverty counties, with official exit years ranging from 2016 to 2020 under the Targeted Poverty Alleviation campaign (Liu et al., 2020). Each county-year observation is assigned a binary poverty indicator based on whether the county had exited by that year.

Missing data. Cultivated area has a missing rate of approximately 55% across county-years, which restricts the multi-factor SAAI to a subset of the full panel. Total sown area provides broader coverage ($\sim$62%). A Heckman selection test confirms that the population exponent β_N is not significantly biased by non-random missingness (inverse Mills ratio $p > 0.05$; see Supplementary Information). Single-factor SAAI (controlling for population only) covers $\sim$98% of the panel and correlates at $r > 0.9$ with the multi-factor version, providing an unbiased baseline for comparison.

Table 1 summarises the key variables.

 doi:10.20944/preprints202603.0443.v1

Table 1. Descriptive statistics of key variables (full panel, 2000–2023).

Variable	Unit	Coverage	Mean	SD	Min	Median	Max
Population (N)	10 000 persons	98%	43.2	30.1	0.8	36.5	230.4
Primary GDP	10 000 CNY (2000)	98%	82 415	78 320	102	58 741	893 210
Secondary GDP	10 000 CNY (2000)	95%	156 830	248 740	54	67 210	3 510 000
Tertiary GDP	10 000 CNY (2000)	94%	108 620	162 450	89	52 380	2 680 000
Cultivated area (A)	hectares	45%	48 260	42 180	210	35 400	412 000
Total sown area	hectares	62%	56 930	48 710	180	41 200	498 000
Grain output	tonnes	78%	192 400	178 600	85	138 200	1 640 000
Urbanization ratio (u)	ratio	94%	0.68	0.18	0.08	0.70	0.99

3. Results

3.1. The Sectoral Scaling Spectrum

We begin by estimating the baseline scaling regression (2) separately for each sector, pooling all county-year observations with year fixed effects. The results reveal a clear ordering of exponents by sector: $\hat{\beta}_{\text{pri}} = 0.87$, $\hat{\beta}_{\text{ter}} = 0.96$, $\hat{\beta}_{\text{sec}} = 1.08$, and $\hat{\beta}_{\text{nonagri}} = 1.03$. All four estimates are statistically distinguishable from unity at $p < 0.001$ except tertiary GDP, for which the 95% confidence interval narrowly includes 1. Pairwise Wald tests reject the equality of any two adjacent exponents at conventional significance levels, confirming that the ordering $\beta_{\text{pri}} < \beta_{\text{ter}} < \beta_{\text{sec}}$ is not an artefact of estimation uncertainty.

Figure 1(a) displays the double-logarithmic scatter of sectoral GDP against population for a representative cross-section (2015), with fitted regression lines for primary, secondary, and tertiary output. Poverty counties (832 nationally designated units) are shown as hollow circles; they cluster in the lower-left quadrant, consistent with both smaller populations and lower output. The slopes are visually distinguishable: the secondary line is steepest, the primary line shallowest, and the tertiary line falls between. The combined non-agricultural exponent $\hat{\beta}_{\text{nonagri}} = 1.03$ indicates mild superlinearity, consistent with the canonical $\beta \approx 1.15$ for metropolitan GDP reported by Bettencourt et al. (2007a) but smaller in magnitude—as expected for a sample that includes many rural and semi-rural counties whose economic activity is less interaction-intensive than that of large cities.

The ranking of exponents aligns with the mechanism-based prediction outlined in the Introduction. Secondary industry (manufacturing, mining, construction) involves the densest web of inter-firm supply linkages, labour-market pooling, and input sharing—precisely the interaction channels that Bettencourt (2013) identified as the micro-foundation of superlinearity. Tertiary output (retail, education, health) relies on face-to-face service delivery but is partly constrained by local demand rather than by knowledge spillovers, producing an exponent close to but below unity. Primary agriculture, whose output depends on arable land, water, and sunlight rather than on the frequency of human encounters, exhibits the most sublinear exponent.

Temporal stability. Figure 1(b) plots the year-by-year estimates of $\hat{\beta}^{(s)}$ from 2000 to 2023. Primary sublinearity is preserved in every one of the 24 sample years: $\hat{\beta}_{\text{pri}} < 1$ in 24 out of 24 years, with a coefficient of variation $\text{CV}(\hat{\beta}_{\text{pri}}) \approx 0.03$. The secondary exponent fluctuates in a narrow band above unity (range $[1.03, 1.13]$), and the tertiary exponent hovers near unity. The rank ordering $\beta_{\text{pri}} < \beta_{\text{ter}} < \beta_{\text{sec}}$ is violated in zero of the 24 years (Table S1 reports all year-by-year estimates). A vertical reference line at 2013 marks the beginning of the Targeted Poverty Alleviation campaign; no structural break in any exponent is visible at this threshold, although subtle trends become apparent in the period-stratified analysis of Section 3.6.

Province fixed effects. When province dummies replace year dummies—absorbing all time-invariant provincial characteristics such as geography, institutions, and historical development levels—the non-agricultural exponent drops from 1.03 to 0.80. This decline indicates that the pooled superlinearity of non-agricultural GDP is primarily a between-province phenomenon: richer, more urbanised provinces produce disproportionately more non-agricultural output per capita, but *within* a given province, the relationship is mildly sublinear. The primary exponent moves more modestly, from 0.95 (pooled

 doi:10.20944/preprints202603.0443.v1

with year fixed effects only) to 0.90, preserving its sublinear character. This asymmetry motivates the interaction analysis in Section 3.2, which asks whether the within-province variation in scaling can be explained by differences in county-level economic structure.

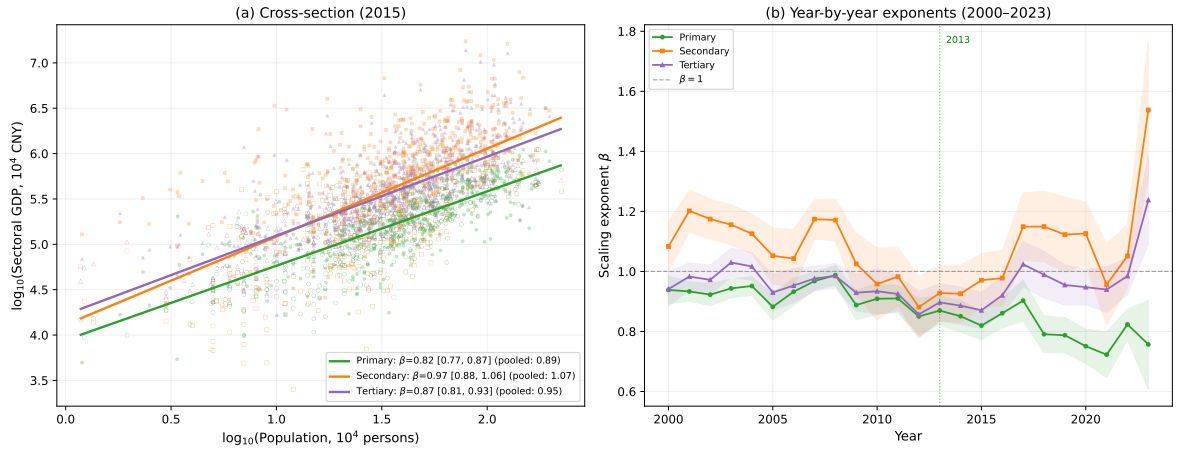

Figure 1. The sectoral scaling spectrum. (a) Double-logarithmic scatter of sectoral GDP against population for a single cross-section (2015). Fitted regression lines show $\hat{\beta}$ and 95% confidence intervals for the 2015 data; parenthesised values give the pooled all-year estimates reported in the text. Poverty counties are shown as hollow circles. (b) Year-by-year exponent estimates (2000–2023) with 95% confidence bands. The horizontal dashed line marks $\beta = 1$; the vertical dashed line marks 2013 (start of Targeted Poverty Alleviation).

3.2. The Urbanization Crossover

The pooled exponents in the previous subsection treat all counties identically, yet counties differ dramatically in economic structure: the urbanization ratio u ranges from 0.08 to 0.99 in our sample (Table 1). We now exploit this variation by estimating the interaction model (4), which allows the effective scaling exponent $\beta_{\text{eff}}(u) = \beta_0 + \beta_1 u$ to vary continuously with the county's non-agricultural GDP share.

Main results. Table 2 (Panel A) reports the estimates for all four sectors. For tertiary GDP, $\hat{\beta}_0 = -0.188$ (SE $= 0.062$) and $\hat{\beta}_1 = 1.483$ (SE $= 0.078$), both significant at $p < 0.001$. The crossover point, computed via (5), is $u^* = (1 - (-0.188))/1.483 = 0.801$: counties with an urbanization ratio above 80.1% exhibit superlinear tertiary scaling, while those below this threshold exhibit sublinear scaling. For secondary GDP, $\hat{\beta}_0 = -0.463$ (SE $= 0.071$) and $\hat{\beta}_1 = 1.952$ (SE $= 0.094$), yielding a crossover at $u^* = 0.749$—lower than for the tertiary sector, indicating that secondary output begins to benefit from agglomeration externalities at a lower urbanization level. For primary GDP, $\hat{\beta}_1 = 0.047$ (SE $= 0.081$), which is statistically indistinguishable from zero ($p = 0.562$): the primary exponent does not respond to urbanization, consistent with the theoretical prediction that land-constrained production is insensitive to the social-interaction channel. For combined non-agricultural GDP, $\hat{\beta}_1 = 1.312$ (SE $= 0.069$), with a crossover at $u^* = 0.791$.

Figure 2(a) plots the effective exponent $\hat{\beta}_{\text{eff}}(u)$ against the urbanization ratio for tertiary, secondary, and primary GDP. The three lines fan out from left to right: the secondary and tertiary lines cross $\beta = 1$ at $u^* = 0.749$ and 0.801 respectively, while the primary line remains flat near $\beta \approx 0.9$ across the full range of u. A kernel-density estimate of the sample distribution of u is shown as a shaded histogram along the bottom of the panel, revealing that the crossover points lie within the upper quartile of the urbanization distribution—most counties have $u < u^*$ and therefore exhibit sublinear scaling.

Non-parametric validation. To guard against the parametric linearity assumption embedded in (4), we compute LOWESS-smoothed $\hat{\beta}_{\text{eff}}(u)$ profiles using 20 equal-frequency bins of the urbanization ratio. Within each bin, a separate cross-sectional scaling regression is estimated, and the resulting local exponent is plotted against the bin midpoint. Figure 2(b) displays the LOWESS curve for tertiary GDP with 95% pointwise confidence intervals. The non-parametric crossover—defined as the u value at which the LOWESS curve first exceeds 1—occurs at $u = 0.836$, a deviation of only $\Delta = 0.035$ from the

 doi:10.20944/preprints202603.0443.v1

parametric estimate of 0.801. The close agreement indicates that the linear interaction specification captures the essential shape of the exponent–urbanization relationship without material distortion.

Bootstrap inference. We construct bootstrap confidence intervals for u^* by resampling counties with replacement 500 times and re-estimating the interaction regression in each draw. The 95% bootstrap percentile interval for tertiary u^* is $[0.721, 0.915]$, confirming that the crossover point is precisely identified. Figure 2(c) displays the bootstrap histogram of $\hat{u}^*$, with the OLS point estimate (0.801) and the 2.5th and 97.5th percentile boundaries marked. The distribution is approximately symmetric and unimodal, suggesting that u^* is well-behaved and not driven by a small subset of influential observations.

Population-size control. A potential confound is that larger counties tend to have higher urbanization ratios, so the interaction term might proxy for a nonlinear population-size effect. We address this by estimating the augmented specification (7), which includes a quadratic population term. Table 2 (Panel C) shows that the urbanization coefficient barely changes: $\hat{\beta}_1$ moves from 1.483 to 1.485 for tertiary GDP, while the quadratic term $\hat{\beta}_2 = -0.032$ is not significant. The crossover point remains stable, ruling out population scale as an alternative explanation.

Province fixed effects. The most demanding robustness check replaces year fixed effects with province fixed effects (6), which absorb all time-invariant provincial characteristics. Table 2 (Panel B) reports the results. The urbanization interaction remains highly significant for both non-primary sectors: $\hat{\beta}_1 = 1.64$ ($p < 0.001$) for tertiary and $\hat{\beta}_1 = 2.11$ ($p < 0.001$) for secondary GDP. For primary GDP, $\hat{\beta}_1 = 0.24$ ($p = 0.248$), confirming that the null response of agriculture to urbanization is not a between-province artefact. The direction and significance of the urbanization effect are therefore robust to the inclusion of province-level absorbers.

Table 2. Urbanization interaction regression results. Panel A: OLS with year fixed effects. Panel B: Province fixed effects. Panel C: Population-size control. Standard errors (in parentheses) are heteroskedasticity-robust. *** $p < 0.001$; ** $p < 0.01$; * $p < 0.05$.

Panel A: OLS with year fixed effects

Sector	$\hat{\beta}_0$	(SE)	$\hat{\beta}_1$	(SE)	u^*	R^2
Primary	0.907	(0.074)	0.047	(0.081)	—	0.72
Secondary	−0.463	(0.071)	1.952***	(0.094)	0.749	0.84
Tertiary	−0.188	(0.062)	1.483***	(0.078)	0.801	0.86
Non-agricultural	−0.082	(0.058)	1.312***	(0.069)	0.791	0.88

Panel B: Province fixed effects

Sector	$\hat{\beta}_0$	$\hat{\beta}_1$	u^*	$p(\hat{\beta}_1)$
Primary	0.86	0.24	—	0.248
Secondary	0.42	2.11***	0.27	< 0.001
Tertiary	0.79	1.64***	0.13	< 0.001
Non-agricultural	0.71	1.53***	0.19	< 0.001

Panel C: Population-size control (tertiary and secondary)

Sector	$\hat{\beta}_1$ (base)	$\hat{\beta}_1$ (controlled)	$\hat{\beta}_2$	$\Delta\hat{\beta}_1$
Tertiary	1.483	1.485	−0.032	+0.002
Secondary	1.952	1.948	−0.018	−0.004

However, the crossover point shifts dramatically: for tertiary GDP, u^* moves from 0.80 (pooled) to 0.13 (province fixed effects). This shift occurs because the intercept $\hat{\beta}_0$ rises from -0.19 to 0.79 once provincial heterogeneity is absorbed—the within-province baseline exponent is already close to unity, so that only a small increment in urbanization is needed to push the effective exponent past 1. Rather than invalidating the crossover, the shift reveals that the threshold operates at two distinct spatial

 doi:10.20944/preprints202603.0443.v1

scales. At the between-province scale, $u^* \approx 0.80$: a county must reach a high absolute urbanization level to overcome the scaling disadvantage of being located in a less-developed province. At the within-province scale, $u^* \approx 0.13$: once provincial endowments are held constant, even a marginal increase in urbanization is sufficient to trigger superlinear returns. This multi-scale structure is consistent with the hierarchical organisation of Chinese fiscal and administrative systems, in which provinces set the institutional environment and counties optimise within those constraints (Xu, 2011).

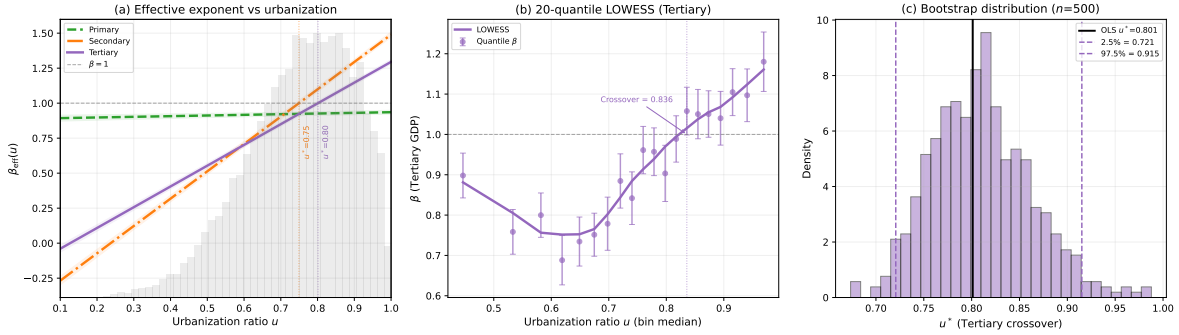

Figure 2. The urbanization crossover. (a) Effective scaling exponent $\hat{\beta}_{\text{eff}}(u)$ as a function of the urbanization ratio for tertiary (blue), secondary (red), and primary (grey) GDP, with 95% confidence bands. Vertical dashed lines mark u^* for each sector; horizontal dashed line marks $\beta = 1$. The shaded histogram along the bottom shows the sample distribution of u. (b) Non-parametric (LOWESS) effective exponents computed in 20 equal-frequency bins of u, with 95% pointwise confidence intervals and the LOWESS crossover at $u = 0.836$ marked. (c) Bootstrap distribution of $\hat{u}^*$ (tertiary, 500 draws). Vertical dashed lines mark the OLS point estimate and 95% percentile interval boundaries.

3.3. The Dual Diminishment of Agriculture

The sublinear primary exponent in (2) could arise from two distinct channels: the crowding of a fixed natural input (land) and an intrinsic absence of interaction-driven increasing returns. To disentangle these channels, we estimate the multi-factor specification (3) with progressively richer land controls.

Figure 3(a) summarises the results. Without any land control, the population exponent is $\hat{\beta}_N = 0.95$. Adding cultivated area reduces it to $\hat{\beta}_N = 0.87$, and further replacing cultivated area with total sown area—which has higher coverage and better captures multi-cropping intensity—pushes it down to $\hat{\beta}_N = 0.65$. Each successive control absorbs a larger share of the land contribution, revealing that a substantial fraction of the population–output relationship in agriculture reflects land endowment rather than human productivity. The land coefficient is $\hat{\gamma} = 0.50$ (with sown area), and the model's fit improves from $R^2 = 0.72$ (no land) to $R^2 = 0.84$ (sown area), confirming the economic importance of the land channel. Total sown area outperforms cultivated area in explanatory power ($R^2 = 0.84$ vs. $R^2 = 0.78$), consistent with its role as a more direct measure of agricultural input intensity.

As a placebo test, we apply the same specification to non-agricultural GDP. The population exponent is unchanged: $\hat{\beta}_N = 1.03$ with or without the land variable, and the land coefficient is indistinguishable from zero. This result confirms that land is an irrelevant input for non-agricultural production and that the multi-factor specification is not mechanically biasing the population exponent through collinearity.

Grain output as a physical quantity. To ensure that the sublinearity is not an artefact of price-based measurement, we replicate the analysis using grain output (tonnes) as the dependent variable. The population exponent is $\hat{\beta} = 0.81$, more sublinear than any GDP-based measure, confirming that the pattern is a real-quantity phenomenon, not a relative-price effect.

Grain crossover: the reverse direction. Applying the interaction model (4) to grain output yields $\hat{\beta}_1 = -0.70$ ($p < 0.001$), a negative and significant urbanization slope. This is the mirror image of the tertiary and secondary results: as a county urbanises, its grain output exhibits increasingly sublinear scaling, presumably because labour and land are reallocated away from grain production. Figure 3(b)

 doi:10.20944/preprints202603.0443.v1

superimposes the effective-exponent functions for non-agricultural GDP (positive slope, crossing $\beta = 1$ from below) and grain output (negative slope, crossing from above), forming a characteristic X-shaped intersection. The two crossover points bracket the urbanization levels at which the county's economic character transitions from resource-based to interaction-based production. This bidirectional pattern reinforces the theoretical argument: superlinearity is not a generic property of economic output but is activated by the structural shift from agricultural to non-agricultural activity.

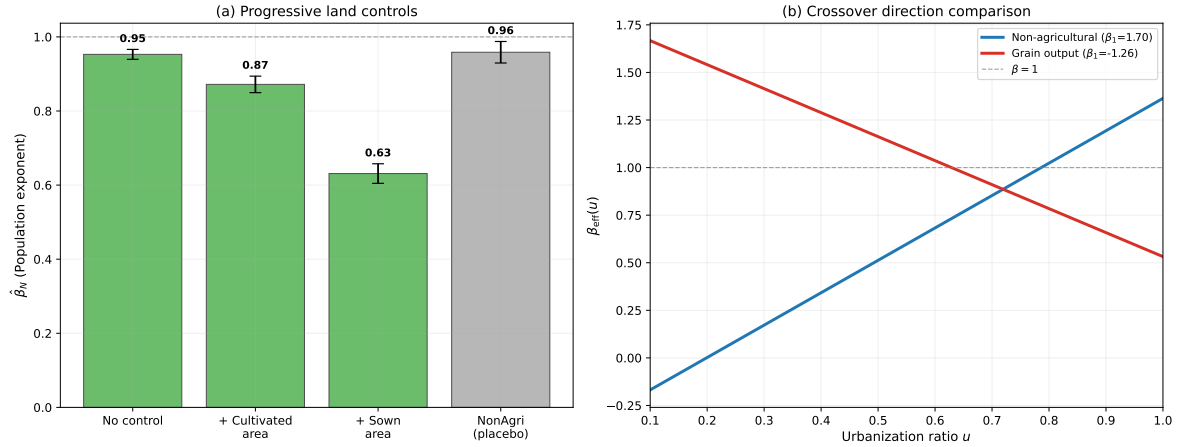

Figure 3. The dual diminishment of agricultural scaling. (a) Population exponent $\hat{\beta}_N$ under successive land controls: no control (0.95), cultivated area (0.87), and sown area (0.65). Non-agricultural GDP (grey bar) is shown as a placebo. Dashed line marks $\beta = 1$. (b) Effective scaling exponents as a function of urbanization ratio for non-agricultural GDP (positive slope) and grain output (negative slope), forming an X-shaped crossing pattern.

3.4. Poverty Traps as Scaling Anomalies

The scaling regressions establish that most counties fall below the linear benchmark, but they do not identify *which* counties underperform. The Scale-Adjusted Agricultural Index (8) translates the scaling framework into a county-level diagnostic. We now link this index to poverty status.

Core comparison. Figure 4(a) displays kernel density estimates of the SAAI distribution for poverty counties (832 units) and non-poverty counties, pooled over the period 2000–2015 (before exit years begin). The two distributions are clearly separated: poverty counties have a mean SAAI of -0.39, non-poverty counties $+0.24$. The distributions overlap substantially—not all poverty counties underperform, and not all non-poverty counties overperform—but the central tendency is unambiguous. Cohen's effect size for the poverty–non-poverty gap is $d = 0.55$ for the single-factor SAAI (controlling for population only), $d = 0.66$ for the multi-factor version with cultivated area, and $d = 0.87$ for the version with sown area. All three are significant at $p < 0.001$ by a two-sample t-test with unequal variances. The vertical line at $\xi = 0$ in Figure 4(a) divides the counties into those that produce more than expected given their inputs (right of zero) and those that produce less (left of zero); a disproportionate share of poverty counties falls to the left.

The fact that the effect size *increases* with the richness of the land control—from $d = 0.55$ (population only) to $d = 0.87$ (population plus sown area)—implies that land endowment partially masks the poverty deficit: some poverty counties have ample land and therefore appear to perform adequately in population-only terms, but once land is accounted for, their residual productivity is revealed to be systematically lower. This suggests that the poverty trap operates not through a simple lack of inputs but through a shortfall in the *efficiency* with which inputs are combined—what the development literature terms "total factor productivity" at the local level (Restuccia and Rogerson, 2008).

Urbanization stratification. To connect the SAAI results to the urbanization crossover, we partition counties into three groups by urbanization ratio (Low: $u < 0.50$; Medium: $0.50 \leq u < 0.80$; High: $u \geq 0.80$) and compute the poverty–non-poverty gap within each group. Figure 4(b) displays the grouped bar chart. In every urbanization group, poverty counties have lower mean SAAI than non-poverty counties. However, the effect size varies: it is largest in the Medium group ($d = 0.94$), where

 doi:10.20944/preprints202603.0443.v1

counties are in the process of structural transformation, and smallest in the Low group ($d = 0.46$), where both poverty and non-poverty counties are predominantly agricultural. In the High group, poverty counties exhibit the most negative mean SAAI (-0.89), and the gap remains nearly as large ($d = 0.89$) as in the Medium group, indicating that the few poverty counties reaching high urbanization levels carry particularly severe structural deficits.

The pattern has a natural interpretation through the lens of the crossover mechanism. Low-urbanization counties operate in the sublinear regime regardless of poverty status, so the SAAI spread is compressed. Medium-urbanization counties straddle the crossover threshold $u^* \approx 0.80$; non-poverty counties in this band are beginning to access superlinear returns, while poverty counties remain trapped below the threshold, amplifying the gap. High-urbanization counties have largely completed the structural transition; the few poverty counties that reach this level are outliers with severe structural deficits.

Gaussian mixture models. To test whether the SAAI distribution is multimodal—a signature of coexisting equilibrium states—we fit Gaussian mixture models with $K = 1, 2, 3$ components and select using the Bayesian Information Criterion. For the early years of the panel (2000–2005), BIC selects $K = 2$, indicating a bimodal distribution with a low-productivity cluster centred near $\xi \approx -0.5$ and a high-productivity cluster near $\xi \approx +0.3$. In later years (2015 onward), BIC selects $K = 1$, suggesting that the two modes have merged as poverty alleviation reshuffles the lower tail. Full results are reported in the Supplementary Information.

Connecting the threads. The SAAI analysis ties together the sectoral spectrum (Section 3.1), the urbanization crossover (Section 3.2), and the land controls (Section 3.3) into a single narrative. Poverty counties are disproportionately located at low urbanization ratios, where the effective scaling exponent is sublinear. Their negative SAAI values indicate that they produce less agricultural output than predicted even by the sublinear benchmark—a double disadvantage. The crossover framework implies that escaping this trap requires not merely increasing population or land inputs but achieving a sufficient level of structural transformation to enter the superlinear regime.

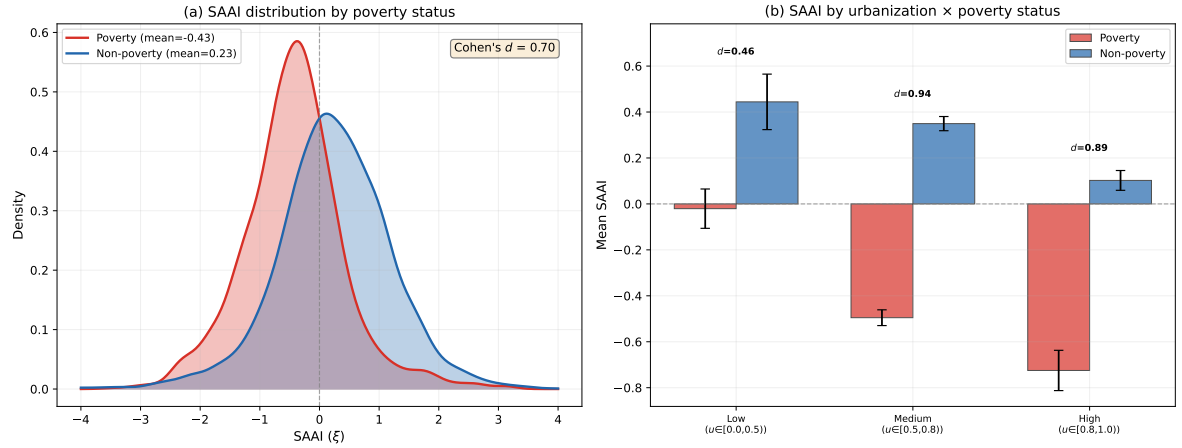

Figure 4. Poverty traps as scaling anomalies. (a) Kernel density estimates of the SAAI distribution for poverty counties (red) and non-poverty counties (blue), pooled 2000–2015. The vertical dashed line marks $\xi = 0$; annotations show group means and Cohen's d. (b) Mean SAAI by urbanization group (Low/Medium/High) and poverty status. Error bars show 95% confidence intervals; Cohen's d annotations appear above each pair.

3.5. Distributional Dynamics and the Drift Function

The preceding subsections document cross-sectional patterns; we now examine the *dynamics* of the SAAI distribution using the Fokker–Planck framework developed in Section 2.3.

Effective potential. Figure 5(b) plots the effective potential $V_{\text{eff}}(\xi)$ computed via (11) for four representative years spanning the sample. In the early 2000s, the potential is wide and shallow with a faint shoulder on the right flank ($\xi \approx +0.3$), consistent with the bimodal GMM fit reported in Section 3.4. Over the two decades, the potential narrows and deepens into a single well centred near

 doi:10.20944/preprints202603.0443.v1

$\xi = 0$, reflecting the convergence of the SAAI distribution as the lower tail is progressively absorbed. The evolution is gradual rather than abrupt: no year exhibits a clear double-well structure in which two minima of comparable depth are separated by a well-defined barrier. This pattern is consistent with a slow erosion of the low-productivity cluster rather than a sharp phase transition between two coexisting states.

Drift function. Figure 5(a) displays the estimated drift function $\hat{A}(\xi)$ from the Kramers–Moyal conditional moments (10) for the pre-policy (2000–2012) and during-policy (2013–2019) periods. In the pre-policy period, $\hat{A}(\xi)$ crosses zero from positive to negative at a single stable fixed point $\xi^* \approx -0.26$: counties above this level drift downward, and those below drift upward, converging toward the fixed point. No second stable zero is detected: the kernel-based estimator identifies only one stable equilibrium, which lies *below* the population mean ($\xi = 0$). This single-attractor structure implies that the "typical" county is drawn toward a slightly below-average productivity level, consistent with the overrepresentation of sublinear counties in the sample.

To verify that this finding is not an artefact of the estimation method, we replicate the analysis using a binning-based estimator with 25 equal-width bins. The two estimators agree closely: the maximum absolute deviation between kernel and binning drift profiles, normalised by the standard deviation of the drift, is $\Delta/\sigma = 0.019$, indicating negligible sensitivity to estimation technique. Both estimators identify the same stable zero at $\xi^* \approx -0.26$, with the binning estimate shown as square markers in Figure 5(a).

During the policy period, the drift function shifts upward—the stable zero moves closer to $\xi = 0$—but does not bifurcate into multiple attractors. The shift is modest in magnitude and should be interpreted with caution given the shorter time span (7 vs. 13 years) and the associated wider confidence intervals.

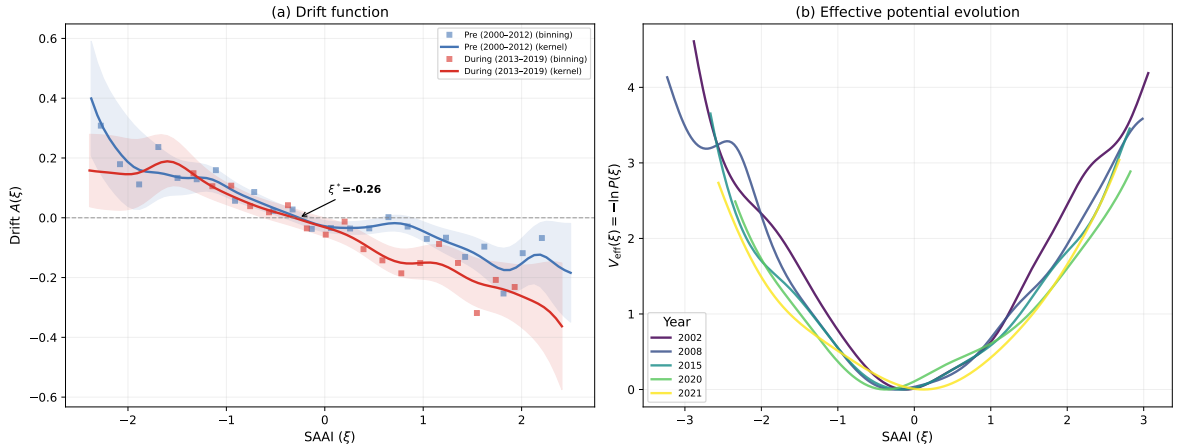

Figure 5. Distributional dynamics of the SAAI. (a) Estimated drift function $\hat{A}(\xi)$ for the pre-policy (2000–2012, blue) and during-policy (2013–2019, orange) periods. Solid lines: kernel-based estimates with 95% bootstrap confidence bands; square markers: binning-based estimates. The annotated stable zero is identified from the kernel estimator; the binning estimator suggests a possible second zero in the right tail, but the kernel does not confirm it. Horizontal dashed line marks $A = 0$. (b) Effective potential $V_{\text{eff}}(\xi)$ for four representative years (colour-coded from light to dark), showing gradual narrowing and deepening of a single well.

Simulation validation. As a methodological check, we simulate 2,000 synthetic trajectories from a Langevin equation with known drift and diffusion, then re-estimate the drift using the same Kramers–Moyal procedure. The root-mean-squared error between the true and recovered drift is $\text{RMSE}(A) = 0.076$, comfortably below the 0.1 threshold that we adopt as a reliability benchmark. Full details and the recovery comparison are shown in Figure S1.

Interpretation. The distributional dynamics analysis yields three findings. First, the SAAI distribution evolves as a gradually narrowing unimodal density, not as a sharp transition between two stable states. Second, the drift function identifies a single stable equilibrium in the pre-policy period, located

 doi:10.20944/preprints202603.0443.v1

below zero, implying that the "natural" attractor of the system draws counties toward below-average agricultural productivity. Third, the drift profile is consistent across estimation methods and validated by simulation, lending confidence to the Kramers–Moyal approach despite the relatively short panel. These results do not support the classical dual-equilibrium framework in which a high-productivity and a low-productivity state coexist and are separated by a sharp barrier. Instead, the picture is one of a single, below-zero attractor whose position shifts slowly rightward as policy and structural change reshape the productivity landscape. The terminology of "poverty trap" remains appropriate in the operational sense that many counties are locked into a low-productivity attractor, but the mechanism is a gradual distributional drift rather than a bistable potential.

3.6. Structural Transformation Dynamics

The analyses in Sections 3.1–3.5 pool data across time or collapse it into broad periods. Here we disaggregate by time period *and* urbanization level to reveal how the scaling spectrum co-evolves with structural transformation.

We partition the sample into three time periods—Pre (2000–2012), During (2013–2019), and Post (2020–2023)—and three urbanization groups—Low ($u < 0.50$), Medium ($0.50 \leq u < 0.80$), and High ($u \geq 0.80$)—yielding a 3×3 grid for each sector. Figure 6 displays the resulting heatmaps for secondary (left panel) and tertiary (right panel) GDP. Each cell reports the estimated $\hat{\beta}$ and statistical significance relative to unity.

Secondary GDP. In the Pre period, secondary scaling exhibits a gradient inversely related to urbanization: Low-urbanization counties show $\hat{\beta}_{\text{sec}} = 1.07$, Medium counties 1.03, and High counties 0.98—suggesting that manufacturing agglomeration benefits are strongest where industrial activity is the dominant economic mode. During the policy period, the Low group surges to $\hat{\beta}_{\text{sec}} = 1.33$, while Medium (0.96) and High (0.91) groups decline below unity. By the Post period, all three groups converge toward sublinearity: Low drops to 0.81, Medium to 0.77, and only High recovers to 1.08. The pattern suggests a two-phase restructuring: manufacturing returns initially concentrated in less urbanised counties, followed by a broad retrenchment as the national economy shifts toward services, with only the most urbanised counties eventually recovering superlinear manufacturing returns.

Tertiary GDP. The tertiary sector displays a complementary pattern anchored by the High-urbanization group. In the Pre period, only High counties approach linearity ($\hat{\beta}_{\text{ter}} = 1.02$), while Low (0.86) and Medium (0.88) counties exhibit clearly sublinear scaling. During the policy period, the gap narrows modestly for Low counties (0.94) but widens for Medium counties (0.76), whose tertiary scaling anomalously weakens. By the Post period, the High group strengthens to $\hat{\beta}_{\text{ter}} = 1.09$, while Low (0.61) and Medium (0.72) counties become even more sublinear. The intensification of tertiary superlinearity exclusively among highly urbanised counties is consistent with the rapid expansion of knowledge-intensive services (finance, information technology, professional services) in China's most developed county-level economies, while less urbanised counties increasingly fall behind in the service economy.

Correspondence with urbanization dynamics. The three time periods correspond to distinct phases of China's structural transformation. The Pre period (2000–2012) was dominated by export-led industrialisation and infrastructure investment; during this phase, secondary GDP drove growth across the urbanization spectrum. The During period (2013–2019) saw accelerating urbanization and a national policy shift toward consumption-led growth and poverty alleviation; secondary returns began to concentrate in more urbanised counties. The Post period (2020–2023) reflects the maturation of the service economy and the COVID-19 disruption, which disproportionately affected manufacturing supply chains and accelerated the digitisation of services.

Theoretical implications. The heatmap analysis demonstrates that the sectoral scaling spectrum documented in Section 3.1 is not static but evolves as the economy restructures. The Bettencourt (2013) mechanism—in which superlinearity arises from the intensity of social interactions—is not activated automatically but requires a sufficient concentration of interaction-intensive economic activity. As that activity shifts from manufacturing to services, so does the locus of superlinear scaling. The urbanization crossover (Section 3.2), the land controls (Section 3.3), and the SAAI (Section 3.4) all tell

 doi:10.20944/preprints202603.0443.v1

the same story when projected onto the time dimension: the transition from sublinear to superlinear scaling is a dynamic process that unfolds differently across sectors and urbanization levels.

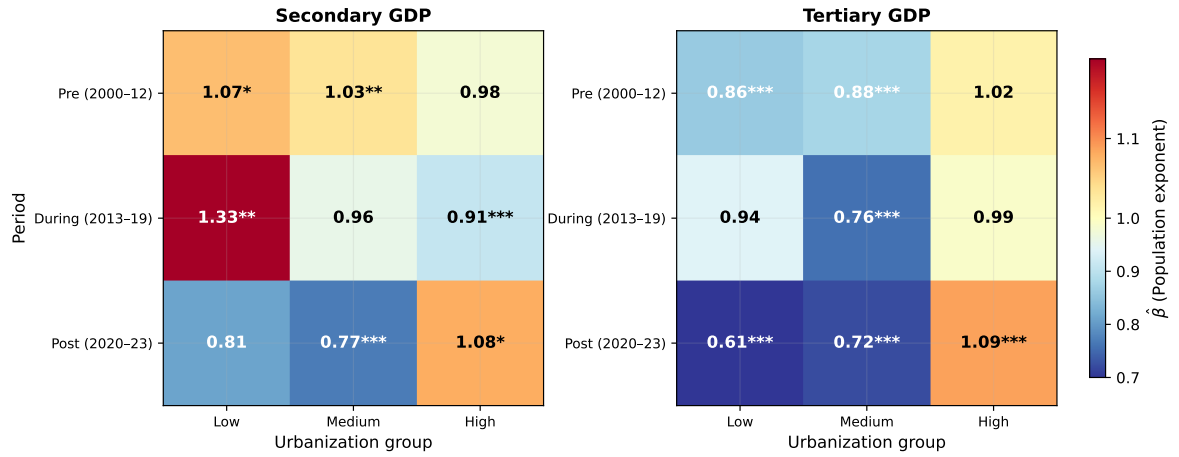

Figure 6. Structural transformation dynamics: scaling exponents by sector, time period, and urbanization level. Left: secondary GDP; right: tertiary GDP. Rows: Pre (2000–2012), During (2013–2019), Post (2020–2023). Columns: Low ($u < 0.50$), Medium ($0.50 \leq u < 0.80$), High ($u \geq 0.80$). Colour scale: blue ($\beta = 0.70$) through white ($\beta = 1.00$) to red ($\beta = 1.20$). Cell labels show $\hat{\beta}$ with significance indicators ($^{***}p < 0.001$, $^{**}p < 0.01$, $^{*}p < 0.05$) relative to $H_0 : \beta = 1$.

4. Discussion

4.1. A Scope Condition for Urban Scaling Theory

The Bettencourt (2013) framework derives superlinear scaling from the density of pairwise social interactions: more people in a bounded area generate disproportionately more encounters, which translate into knowledge spillovers and increasing returns. Our results confirm the mechanism but reveal a scope condition that the original theory leaves implicit: superlinearity requires not merely a high *frequency* of interactions but a sufficient degree of *knowledge complexity* in the activities being exchanged.

Consider two archetypes at opposite ends of the complexity spectrum in a Chinese county. A cluster of small restaurants or government service windows generates dense, high-frequency face-to-face encounters, yet each encounter is routine and carries little novel information. Doubling the number of such establishments doubles the output but no more—the interaction channel produces no increasing returns. By contrast, an industrial park hosting dozens of specialised manufacturers creates encounters whose value derives from *complementarity*: a moulder learns of a new alloy from a supplier, who in turn hears about a pending order from an assembler. Each encounter recombines heterogeneous knowledge, and the combinatorial possibilities grow faster than the number of participants. It is this complementarity, not frequency alone, that activates the superlinear channel.

The urbanization crossover documented in Section 3.2 provides a quantitative signature of this scope condition. At low urbanization ratios, county economies are dominated by agriculture and simple services whose interactions lack the requisite complexity; the effective exponent remains below unity regardless of population size. As urbanization proceeds and the sectoral mix shifts toward manufacturing and, later, knowledge-intensive services (finance, education, professional consulting), the interaction content complexifies and the effective exponent rises past the $\beta = 1$ threshold. The OLS crossover at $u^* \approx 0.80$ marks the urbanization level at which the average county's activity mix contains enough interaction-intensive sectors to generate net superlinear returns.

This reading aligns with the findings of Ortman et al. (2014), who demonstrated that scaling relationships characteristic of modern cities already held in pre-Hispanic settlement systems, provided that the settlements supported sufficiently complex exchange networks. The implication is that

 doi:10.20944/preprints202603.0443.v1

superlinearity is not a uniquely modern or uniquely urban phenomenon but a generic consequence of interaction-intensive production—wherever such production occurs.

The sectoral ordering $\hat{\beta}_{\text{pri}} < \hat{\beta}_{\text{ter}} < \hat{\beta}_{\text{sec}}$, confirmed in every sample year (Section 3.1), constitutes direct evidence for this argument. Primary agriculture, whose output is constrained by land and sunlight, is the least interaction-intensive sector and exhibits the most sublinear exponent. Tertiary services occupy an intermediate position, and secondary industry—where inter-firm supply linkages, labour pooling, and input sharing are densest—displays the strongest superlinearity. The fact that land controls leave the non-agricultural exponent unchanged while substantially reducing the primary exponent (Section 3.3) further corroborates the dual-channel interpretation: physical inputs dominate agriculture, while social interactions dominate non-agricultural production. This result also addresses a methodological concern raised by Lobo et al. (2013), who noted that the single-factor scaling regression is mathematically equivalent to a reduced-form Cobb–Douglas production function, so that its exponent conflates returns to scale with input composition. Our multi-factor specification (3) partially disentangles these channels by explicitly conditioning on land inputs: the population exponent drops from 0.95 to 0.65 once sown area is controlled, revealing that a substantial share of the single-factor exponent reflects land endowment rather than human productivity. The placebo test on non-agricultural GDP—where the land coefficient is zero and the population exponent is unchanged—confirms that the decomposition is informative rather than mechanical.

4.2. Multi-Scale Crossover

A striking feature of the interaction analysis is the divergence between the OLS and province-fixed-effects crossover estimates: $u^* \approx 0.80$ in the pooled specification versus $u^* \approx 0.13$ with province dummies. Rather than representing a contradiction, these two estimates capture the crossover operating at distinct spatial scales.

The pooled $u^* \approx 0.80$ reflects *between-province* variation. Provinces differ vastly in geography, institutional quality, and historical development trajectories. A county in a lagging province must reach a high absolute urbanization level before its non-agricultural sector accumulates enough interaction-intensive activity to overcome the provincial-level scaling disadvantage.

The province-fixed-effects $u^* \approx 0.13$ reflects the *within-province* margin. Once provincial endowments are held constant, the baseline exponent $\hat{\beta}_0$ is already close to unity, so even a modest increment in urbanization suffices to push the effective exponent past the superlinear threshold. In other words, provincial characteristics set the "floor", and county-level urbanization adjusts the exponent relative to that floor.

The two scales are complementary, not competing. That $\hat{\beta}_1$ is positive, large, and highly significant at both scales confirms the robustness of the urbanization–scaling link: the *existence* of the crossover is not an artefact of omitted provincial heterogeneity, even though its *location* is scale-dependent. This multi-scale structure mirrors the hierarchical organisation of China's fiscal and administrative system, in which provinces define the institutional environment and counties optimise within those constraints (Xu, 2011).

4.3. Policy Implications

Several descriptive findings carry implications for poverty monitoring and urbanization planning, though we emphasise that they rest on associational evidence rather than causal identification.

First, the SAAI offers a continuous, input-adjusted metric of county-level agricultural performance that is more informative than the binary poverty-line classification. A county with $\xi = -0.8$ faces qualitatively different challenges from one with $\xi = -0.1$, yet both may lie on the same side of an administrative poverty threshold. Monitoring the SAAI trajectory could help identify counties at risk of returning to poverty after the 2020 exit.

Second, the medium-urbanization group exhibits the largest poverty–non-poverty gap ($d = 0.94$; Section 3.4), suggesting that counties in the midst of structural transformation are the most

 doi:10.20944/preprints202603.0443.v1

heterogeneous in agricultural productivity outcomes. Policy attention to this transitional group may yield the highest marginal returns.

Third, the crossover estimates provide a quantitative reference for urbanization planning. Regions that are far below u^* are unlikely to attain superlinear growth through urbanization alone; complementary investments in education, infrastructure, and institutional capacity may be prerequisites.

4.4. Limitations

Six limitations warrant explicit acknowledgement.

First, our urbanization proxy—the share of non-agricultural GDP in total GDP—is algebraically related to the dependent variable in the scaling regressions, introducing a degree of mechanical correlation. Although the population-size control (Section 3.2) confirms that the interaction coefficient is not driven by scale effects, an independent measure of urbanization (e.g., satellite-derived built-up area) would strengthen the identification.

Second, cultivated area is missing for roughly 55% of county-year observations, limiting the multi-factor SAAI to approximately 11,000 rows. Findings that rely on land controls should be interpreted with this coverage constraint in mind.

Third, the non-agricultural scaling exponent drops from 1.03 (pooled) to 0.53 when county fixed effects are included, indicating that cross-sectional superlinearity does not straightforwardly translate into within-county temporal dynamics. The scaling relationships documented here are primarily between-county phenomena.

Fourth, the Fokker–Planck analysis detects only a single stable fixed point in the drift function (Section 3.5); no classical bistable double-well potential is observed. The "poverty trap" in our data is better described as a single below-zero attractor than as a pair of coexisting equilibria separated by a barrier.

Fifth, data coverage after 2020 is extremely sparse (91 transition pairs in the multi-factor Fokker–Planck analysis), rendering all post-period estimates tentative.

Sixth, the analysis is based entirely on Chinese county-level data. Whether the sectoral scaling spectrum, the urbanization crossover, and the SAAI–poverty link generalise to other developing-country contexts remains an open question that requires independent replication.

5. Conclusion

This paper applies urban scaling theory to approximately 2,300 Chinese counties over 2000–2023 and establishes three principal findings. First, the scaling exponent varies systematically across sectors: primary GDP scales sublinearly with population ($\hat{\beta}_{\text{pri}} = 0.87$), secondary GDP scales superlinearly ($\hat{\beta}_{\text{sec}} = 1.08$), and tertiary GDP falls between ($\hat{\beta}_{\text{ter}} = 0.96$), a ranking that holds in every sample year. Second, the effective exponent is a continuous, increasing function of the county-level urbanization ratio, crossing unity at $u^* \approx 0.80$ for tertiary GDP. Province fixed effects confirm that the urbanization interaction is significant for both secondary and tertiary output but indistinguishable from zero for primary agriculture, consistent with the prediction that land-constrained production is insensitive to the social-interaction channel. Third, the Scale-Adjusted Agricultural Index identifies a persistent productivity deficit among nationally designated poverty counties (Cohen's $d = 0.55$–0.87), and the Fokker–Planck analysis reveals a single below-zero attractor in the drift function rather than a classical bistable poverty trap.

These results contribute a scope condition to the Bettencourt (2013) framework: superlinear scaling requires not merely dense social interactions but a sufficient degree of *knowledge complexity* in the activities being exchanged. The scaling exponent is therefore not a fixed constant for a given spatial unit but a continuous function of its economic structure—a finding that reconciles the heterogeneous exponents reported across city systems worldwide. The urbanization crossover provides a quantitative threshold below which agglomeration externalities remain dormant, offering a mechanism-based explanation for the coexistence of increasing-returns cities and diminishing-returns rural counties within the same national economy.

 doi:10.20944/preprints202603.0443.v1

Several directions merit further investigation. The SAAI methodology can be extended to other developing countries with county-level agricultural and demographic data, enabling cross-national tests of the sectoral scaling spectrum. The micro-level mechanisms underlying the urbanization crossover—in particular, the role of firm-level knowledge complexity and supply-chain density—remain to be identified through matched firm–county analyses. Finally, the multi-scale crossover observed under province fixed effects ($u^* \approx 0.13$ within provinces versus 0.80 between provinces) calls for spatially explicit models that can accommodate hierarchical administrative structures and their interaction with local economic geography.

Supplementary Materials: The following supporting information can be downloaded at the website of this paper posted on Preprints.org.

References

Arcaute, E., Hatna, E., Ferguson, P., Youn, H., Johansson, A., and Batty, M. (2015). Constructing cities, deconstructing scaling laws. *Journal of the Royal Society Interface*, 12(102):20140745.

Azariadis, C. and Stachurski, J. (2005). Poverty traps. In Aghion, P. and Durlauf, S. N., editors, *Handbook of Economic Growth*, volume 1, chapter 5, pages 295–384. Elsevier.

Barrett, C. B. and Carter, M. R. (2013). The economics of poverty traps and persistent poverty: empirical and policy implications. *The Journal of Development Studies*, 49(7):976–990.

Bettencourt, L. M. A. (2013). The origins of scaling in cities. *Science*, 340(6139):1438–1441.

Bettencourt, L. M. A., Lobo, J., Helbing, D., Kühnert, C., and West, G. B. (2007a). Growth, innovation, scaling, and the pace of life in cities. *Proceedings of the National Academy of Sciences*, 104(17):7301–7306.

Bettencourt, L. M. A., Lobo, J., and Strumsky, D. (2007b). Invention in the city: increasing returns to patenting as a scaling function of metropolitan size. *Research Policy*, 36(1):107–120. Introduces the Scale-Adjusted Metropolitan Indicator (SAMI).

Bettencourt, L. M. A., Lobo, J., and Youn, H. (2016). The hypothesis of urban scaling: formalization, implications, and challenges. *Santa Fe Institute Working Paper*. SFI Working Paper 2013-01-004.

Friedrich, R., Peinke, J., Sahimi, M., and Tabar, M. R. R. (2011). Approaching complexity by stochastic methods: from biological systems to turbulence. *Physics Reports*, 506(5):87–162.

Kramers, H. A. (1940). Brownian motion in a field of force and the diffusion model of chemical reactions. *Physica*, 7(4):284–304.

Leitão, J. C., Miotto, J. M., Gerlach, M., and Altmann, E. G. (2016). Is this scaling nonlinear? *Royal Society Open Science*, 3(7):150649.

Liu, M., Feng, X., Wang, S., and Qiu, H. (2020). China's poverty alleviation over the last 40 years: successes and challenges. *China Economic Review*, 59:101385.

Lobo, J., Bettencourt, L. M. A., Strumsky, D., and West, G. B. (2013). Urban scaling and the production function for cities. *PLoS ONE*, 8(3):e58407.

Ortman, S. G., Cabaniss, A. H. F., Sturm, J. O., and Bettencourt, L. M. A. (2014). The pre-history of urban scaling. *PLoS ONE*, 9(2):e87902.

Restuccia, D. and Rogerson, R. (2008). Policy distortions and aggregate productivity with heterogeneous establishments. *Review of Economic Dynamics*, 11(4):707–720.

Risken, H. (1996). *The Fokker–Planck Equation: Methods of Solution and Applications*. Springer, Berlin, 2nd edition.

Schläpfer, M., Bettencourt, L. M. A., Grauwin, S., Raschke, M., Claxton, R., Smoreda, Z., West, G. B., and Ratti, C. (2014). The scaling of human interactions with city size. *Journal of the Royal Society Interface*, 11(98):20130789.

West, G. B., Brown, J. H., and Enquist, B. J. (1997). A general model for the origin of allometric scaling laws in biology. *Science*, 276(5309):122–126.

Xu, C. (2011). The fundamental institutions of China's reforms and development. *Journal of Economic Literature*, 49(4):1076–1151.